Catalysis Today 151 (2010) 362–375

Contents lists available at ScienceDirect

Catalysis Today

journal homepage: www.elsevier.com/locate/cattod

NO_x storage–reduction characteristics of Ba-based lean NO_x trap catalysts subjected to simulated road aging

Yaying Ji [a], Courtney Fisk [a], Vencon Easterling [a], Uschi Graham [a], Adam Poole [a], Mark Crocker [a,*], Jae-Soon Choi [b], William Partridge [b], Karen Wilson [c]

[a] Center for Applied Energy Research, University of Kentucky, 2540 Research Park Drive, Lexington, KY 40511-8479, USA
[b] Fuels, Engines, and Emissions Research Center, Oak Ridge National Laboratory, 2360 Cherahala Blvd., Knoxville, TN 37932-1563, USA
[c] Department of Chemistry, University of York, Heslington, York, YO10 5DD, UK

ARTICLE INFO

Article history:
Available online 18 January 2010

Keywords:
Lean NO_x trap
NO_x storage
Catalyst aging
Precious metal sintering
Ceria

ABSTRACT

In order to study the effect of washcoat composition on lean NO_x trap (LNT) aging characteristics, fully formulated monolithic LNT catalysts containing varying amounts of La-stabilized CeO_2 (5 wt% La_2O_3) or CeO_2-ZrO_2 (Ce:Zr = 70:30) were subjected to accelerated aging on a bench reactor. Subsequent catalyst evaluation revealed that aging resulted in deterioration of the NO_x storage, NO_x release and NO_x reduction functions, whereas the observation of lean phase NO_2 slip for all of the aged catalysts indicated that LNT performance was not limited by the kinetics of NO oxidation. After aging, all of the catalysts showed increased selectivity to NH_3 in the temperature range 250–450 °C. TEM, H_2 chemisorption, XPS and elemental analysis data revealed two main changes which can explain the degradation in LNT performance. First, residual sulfur in the catalysts, present as $BaSO_4$, decreased catalyst NO_x storage capacity. Second, sintering of the precious metals in the washcoat was observed, which can be expected to decrease the rate of NO_x reduction. Additionally, sintering is hypothesized to result in segregation of the precious metal and Ba phases, resulting in less efficient NO_x spillover from Pt to Ba during NO_x adsorption, as well as decreased rates of reductant spillover from Pt to Ba and reverse NO_x spillover during catalyst regeneration. Spectacular improvement in LNT durability was observed for catalysts containing CeO_2 or CeO_2-ZrO_2 relative to their non-ceria containing analog. This was attributed to (i) the ability of ceria to participate in NO_x storage/reduction as a supplement to the main Ba NO_x storage component; (ii) the fact that Pt and CeO_2(-ZrO_2) are not subject to phase segregation; and (iii) the ability of ceria to trap sulfur, resulting in decreased sulfur accumulation on the Ba component.

1. Introduction

Lean NO_x traps (LNTs) represent a promising technology for the abatement of NO_x under lean conditions [1,2]. LNT catalysts typically contain precious metals (generally Pt and Rh) and an alkali or alkaline earth metal storage component (most commonly BaO) supported on a high surface area metal oxide. Under lean exhaust conditions, NO is oxidized to NO_2 over the precious metal sites in the catalyst and reversibly stored as nitrates or nitrites on the storage material. Stored NO_x species are subsequently released and reduced to N_2 during short periodic excursions to rich (i.e., net reducing) conditions. Although LNTs are starting to find commercial application, the issue of catalyst durability remains problematic. LNT susceptibility to sulfur poisoning is the single most important factor determining effective catalyst lifetime. The NO_x storage element of the catalyst has a greater affinity for SO_3 than it does for NO_2, and the resulting sulfate is more stable than the stored nitrate [3–9]. Although this sulfate can be removed from the catalyst by means of high temperature treatment under rich conditions [10–14], the required conditions give rise to deactivation mechanisms such as precious metal sintering, total surface area loss, and solid state reactions between the various oxides present in the washcoat [15–26]. On the other hand, incomplete removal of sulfur during desulfation can be expected to result in decreased NO_x storage capacity and hence lower NO_x conversion efficiency.

Precious metal sintering has been recognized as a key issue in LNT catalyst durability. Indeed, several studies have suggested that Pt sintering can result in decreased interaction between the Pt and Ba phases (i.e., phase segregation) which can degrade NO_x storage and regeneration behavior [15–25]. Another effect associated with thermal aging is the occurrence of reactions between the storage material and the support, resulting in the formation of Ba aluminate, cerate, zirconate, etc., as appropriate [15–20,26]. Fekete et al. [15] were among the first to attribute the observed decrease in NO_x storage capacity after aging to the formation of mixed metal

* Corresponding author. Tel.: +1 859 257 0295; fax: +1 859 257 0302.
E-mail address: crocker@caer.uky.edu (M. Crocker).

0920-5861/$ – see front matter © 2009 Elsevier B.V. All rights reserved.
doi:10.1016/j.cattod.2009.12.009

oxides from unwanted side reactions between the storage material and the support, in addition to substantial loss of interface between the precious metals and the storage material. It was suggested that the loss of interface leads to a reduced spillover rate of NO_2 from the precious metal to the adsorbent, thereby decreasing NO_x storage efficiency. Uy et al. [16] characterized fresh and aged $Pt/Ba/Al_2O_3$ catalysts using in situ UV and visible Raman spectroscopy and found evidence for Ba particles "separating from" or behaving independently from the Pt/Al_2O_3 in aged $Pt/Ba/Al_2O_3$.

From studies with $Pt\text{-}Ba/Al_2O_3$ catalysts, Jang et al. [26] emphasized the importance of Ba–Al mixed oxide formation as a cause of degraded NO_x storage capacity. Upon heating $Pt\text{-}Ba/Al_2O_3$ from 550 to 850 °C, they observed the gradual conversion of Ba/Al_2O_3 to $BaAl_2O_4$. Several other authors have similarly found that $BaAl_2O_4$ forms at about 850 °C [16–19]. Casapu et al. [17] have studied LNT catalysts that use CeO_2 as a support and found rather similar results, $BaCeO_3$ being reported to form at 800 °C. Although $BaCeO_3$ forms much faster than $BaAl_2O_4$, it decomposes in the presence of CO_2, NO_x, and water at 300–500 °C. In comparison, $BaAl_2O_4$ is much more stable under typical operating conditions but can be converted to $BaCO_3$ and Al_2O_3 at room temperature in the presence of water [19,27].

In an effort to overcome the adverse effects associated with LNT sulfation, considerable effort has been made to enhance the sulfur tolerance of Ba-based LNTs and decrease required desulfation temperatures. The approaches reported to date have included modification of the Ba-based NO_x storage component [28,29], the use of acidic support materials [30,31], as well as the use of alternative NO_x storage materials [4,32–34]. As reported by Theis et al. [35] and by ourselves [36,37], the addition of ceria also improves the tolerance of Ba-based LNTs to sulfur. From monolith studies [37], it was found that relative to a sample containing no ceria, samples containing La-stabilized CeO_2 or $CeO_2\text{-}ZrO_2$ showed greater resistance to deactivation during sulfation (as reflected by the NO_x storage efficiency), and required lower desulfation temperatures to restore the NO_x storage efficiency to its pre-sulfation value. These findings can be attributed in large part to the ability of ceria to store sulfur—thereby helping to protect the Ba phase from extensive sulfation—and release it at relatively low temperatures under reducing conditions.

To understand the effect of ceria on the durability of Ba-based catalysts, we have extended our studies to include catalysts subjected to simulated road aging. The approach utilized makes use of detailed characterization of catalysts (which are compositionally well defined), both prior to and after aging, in tandem with measurement of catalyst performance in NO_x storage and reduction. In this manner, NO_x storage and reduction characteristics can be correlated with the evolution of catalyst microstructure upon aging.

Table 1
Composition of catalysts subjected to simulated road aging.

Component	Catalyst code/loading[a]			
	30-0	30-50	30-100	30-100Z
Pt, g/L (g/cuft)	3.53 (100)	3.53 (100)	3.53 (100)	3.53 (100)
Rh, g/L (g/cuft)	0.71 (20)	0.71 (20)	0.71 (20)	0.71 (20)
BaO, g/L	30	30	30	30
CeO_2[b], g/L	0	50	100	0
$CeO_2\text{-}ZrO_2$, g/L	0	0	0	100
Al_2O_3[c], g/L	Balance	Balance	Balance	Balance

[a] Nominal loadings. Total washcoat loading = 260 g/L.
[b] Stabilized with 5 wt% La_2O_3.
[c] Stabilized with 3 wt% La_2O_3.

2. Experimental

2.1. Catalyst preparation

Four fully formulated Ba-based LNT catalysts were used in this study. Details of the catalyst preparation have been described elsewhere [38]. Briefly, the powders for washcoating were prepared using the incipient wetness method. $Pt(NH_3)_4(OH)_2$ and $Rh(NO_3)_3$ were co-impregnated onto a 3 wt% La_2O_3-stabilized γ-alumina (Sasol Puralox SCFa-140 L3, BET surface area of 140 m^2/g) to give a loading of 2.35 wt% Pt and 2.35 wt% Rh after calcination at 500 °C for 2 h. $Ba(O_2CCH_3)_2$ was impregnated onto γ-alumina (Sasol Puralox SCFa-140 L3) to give a loading of 21 wt% BaO after calcination at 500 °C for 2 h, after which the BaO/Al_2O_3 material was ball milled with the required amount of CeO_2 or $CeO_2\text{-}ZrO_2$. To achieve the total Pt loading, the balance of the Pt was then impregnated onto the above physical mixture using $Pt(NH_3)_4(OH)_2$ precursor, after which it was calcined at 500 °C for 2 h. To prepare the washcoat, 30 g/L of the $Pt\text{-}Rh/Al_2O_3$ powder was slurried in deionized water with the $Pt/[BaO/Al_2O_3 + CeO_2$ (or $CeO_2\text{-}ZrO_2)]$ mixture to which γ-alumina powder was added as balance to achieve a nominal washcoat loading of 260 g/L. Additionally, a small amount of boehmite sol (6 g/L) was added to the washcoat as a binder during preparation of the slurry. As shown in Table 1, these four catalysts have the same nominal loadings of BaO (30 g/L), Pt (3.53 g/L) and Rh (0.71 g/L), while the amount of CeO_2 (or $CeO_2\text{-}ZrO_2$) was varied as indicated. In all cases, the washcoat was applied to a 4 in. × 6 in. cordierite monolith substrate, possessing a cell density of 400 cpsi and a wall thickness of 6.5 mil.

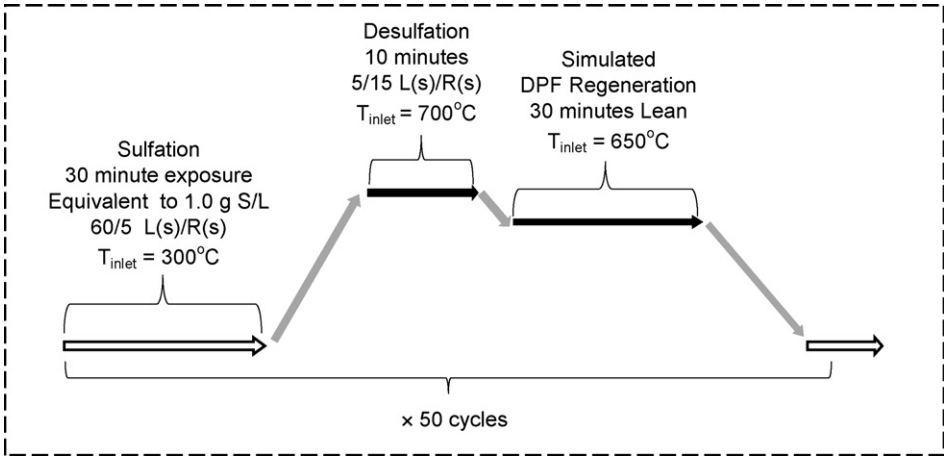

Fig. 1. Summary of protocol used for accelerated catalyst aging.

2.2. Aging protocol

The rapid aging protocol used was based on one developed by Ford Motor Co. [39], and is designed to simulate the road aging of a LNT catalyst used in conjunction with a diesel particulate filter (DPF). As shown in Fig. 1, each aging cycle is composed of three modes: sulfation, desulfation, and simulated DPF regeneration. For the sulfation mode, the gas composition used corresponded to that shown in Table 2, 45 ppm SO_2 being added in the lean and rich phases. The same gas composition was used in the desulfation mode, with the exception that SO_2 was omitted from the feed (both phases). For the third phase, constant lean conditions were used, corresponding to the lean phase gas composition indicated in Table 2. For each mode, the furnace temperature was regulated based on the gas temperature at the front face of the catalyst (i.e., the inlet), since this provided for more stable operation than using the catalyst mid-bed temperature. Fig. 2 shows the mid-bed temperature profile recorded for catalyst 30–50 during the highest temperature portion of the cycle, i.e., the desulfation mode. For each catalyst, the recorded mid-bed temperature in this mode was typically 70 ± 10 °C higher than the 700 °C set-point due to the exotherm created by the fast lean-rich cycling (5 s lean, 15 s rich). In contrast, for the simulated DPF regeneration mode, in which constant lean conditions were applied, the inlet and mid-bed temperatures showed no discrepancy.

Depending on actual fuel sulfur levels, one aging cycle is estimated to be equivalent to 1000–1500 miles of road aging. Fifty cycles were used for the aging runs, requiring a total aging time of ca. 100 h per sample (the cycle time being ca. 2 h). At the end of each aging run a final desulfation was performed under constant rich conditions, corresponding to 2% H_2 in the presence of 5% H_2O and 5% CO_2 at 750 °C for 10 min, in order to remove as much residual sulfur as possible.

2.3. Catalyst evaluation

Catalyst evaluation was performed on a synthetic gas bench reactor. A 2.1 cm diameter and 7.4 cm long core drilled out from each LNT monolith was wrapped in Zetex insulation tape and inserted into a horizontal quartz reactor tube (2.2 cm inner diameter). The reactor tube was heated by an electric furnace, and simulated exhaust gas mixtures were introduced from pressurized gas bottles (ultra high purity grade, Air Liquide). The gases were metered with mass flow controllers (Unit Instruments Series 7300, Kinetics Electronics) and pre-heated before entering the quartz reactor. Water was introduced by a peristaltic cartridge pump (Cole-Parmer) to a heated zone, vaporized and added to the simulated exhaust mixture. A rapid switching 4-way valve system was used to alternate between the lean and rich gas mixtures so that the lean/rich/lean transitions in these experiments were almost instantaneous (within 0.2 s). Three K-type thermocouples were placed just before the LNT, at the LNT mid-point and just after the LNT to monitor the temperature profiles. A multi-gas analyzer (MKS Model 2030 HS) was used to monitor NO, NO_2, N_2O, NH_3, CO, CO_2 and H_2O at the reactor outlet. Determination of intra-catalyst hydrogen concentrations during oxygen storage capacity (OSC) measurements was performed using SpaciMS (spatially resolved capillary inlet mass spectrometry) [40,41] with a removable capillary probe inserted into the channel of the core sample near the centerline. The activity evaluation and OSC measurements for the aged catalysts were performed under the same conditions used previously for the fresh samples (see Table 2) [38]. During the cycling conditions described in Table 2, the observed catalyst breakthrough profiles stabilized to a fixed limit cycle in about 2 h, at which point it was possible to characterize the performance in terms of the 'stationary' concentration cycles. The selectivity to N_2 during the rich purge was determined by difference (i.e., $S_{N_2} = 100\% - S_{N_2O} - S_{NH_3}$).

Table 2
Gas compositions used for rapid aging, oxygen storage–reduction and NO_x storage–reduction cycling experiments.

Parameter	Oxygen storage–reduction cycling and rapid aging		NO_x storage–reduction cycling	
	Lean	Rich	Lean	Rich
Duration, s	60[a]	5[a]	60	5
Space velocity, h^{-1}	30,000	30,000	30,000	30,000
NO, ppm	0 (300[b])	0 (300[b])	300	0
SO_2, ppm	0 (45[c])	0 (45[c])	0	0
O_2, %	10	0	10	0
H_2, %	0	4.2 (1.3[d])	0	1.575
CO, %	0	0 (4[d])	0	2.625
H_2O, %	5	5	5	5
CO_2, %	5	5	5	5
N_2, %	Balance	Balance	Balance	Balance

[a] Duration of lean and rich phases in rapid aging as shown in Fig. 1.
[b] Feed gas for all rapid aging modes contained 300 ppm NO in addition to other components listed.
[c] Feed gas for rapid aging sulfation mode contained 45 ppm SO_2 (lean and rich) in addition to other components listed.
[d] Rich feed gas during rapid aging contained 1.3% H_2 and 4% CO.

2.4. N_2 physisorption

Surface area and pore volume measurements were performed according to the BET method by nitrogen adsorption at −196 °C using a Micromeritics Tri-Star system. Prior to the measurements, catalyst samples (washcoat and monolith) were ground to a fine powder and outgassed overnight at 160 °C under vacuum.

2.5. Pulsed H_2 chemisorption

The dispersion of precious metal (Pt + Rh) was determined with a Micromeritics AutoChem II Analyzer by means of pulsed H_2 chemisorption at dry ice temperature (−78 °C). This temperature was chosen in an effort to minimize H spillover from the metal to the support material [42]. 1 g of sample (as a fine powder), including both washcoat and substrate, was loaded into the reactor. After being oxidized at 400 °C in 10% O_2/He for 15 min, followed by reduction at 300 °C in 10% H_2/Ar for 15 min, the catalyst was heated up to 400 °C (hold time 10 min) in flowing Ar to remove adsorbed H. Pulsed H_2 chemisorption was initiated using a four-way valve after the catalyst had been cooled to −78 °C. During this measurement, 0.5 ml of 10% H_2/Ar was pulsed into the reactor every 2 min, the H_2 signal at the reactor outlet being monitored with a thermal conductivity detector (TCD). H_2 pulsing was terminated after the TCD signal had reached a constant value,

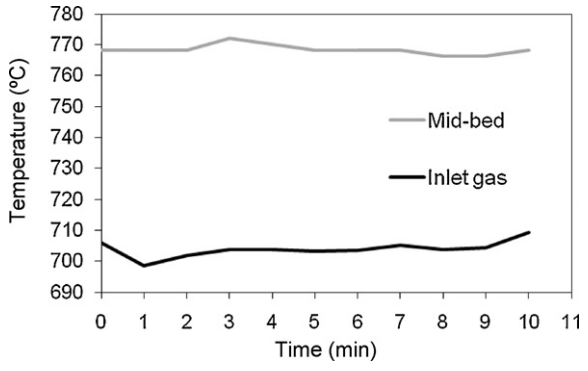

Fig. 2. Mid-bed temperature of catalyst 30-50 during rapid aging desulfation mode.

Table 3
Physical properties of fresh and aged catalysts.

Catalyst	Estimated washcoat BET surface area (m^2/g)[a]		Total BET surface area (m^2/g)		Pore volume (cm^3/g)		Average pore radius (nm)		PM dispersion–chemisorption (%)	
	Fresh	Aged	Fresh	Aged	Fresh	Aged	Fresh	Aged	Fresh	Aged
30-0	121	107	43.5	37.8	0.148	0.137	6.82	7.23	34.0	8.5
30-50	126	88	47.5	32.7	0.156	0.120	6.56	7.35	51.2	9.2
30-100	106	86	41.9	33.4	0.133	0.121	6.35	7.25	57.2	15.1
30-100Z	140	74	54.7	28.4	0.176	0.119	6.44	8.42	45.5	9.2

[a] Estimate calculated from washcoat loading and surface area of 1 m^2/g for cordierite substrate.

i.e., the precious metal (Pt + Rh) sites were saturated with H_2. Assuming a 1:1 ratio of atomic hydrogen to surface Pt or Rh, the metal dispersion was calculated based on the amount of H adsorbed.

2.6. HRTEM–EELS

Material for electron microscopy (EM) analysis, including TEM, STEM, EDS and EELS, was obtained by scraping a small amount of washcoat from the catalyst samples which was supported on TEM grids. High-resolution transmission electron microscopy (HR-TEM) and scanning transmission electron microscopy (STEM) investigations were conducted using a field emission JEOL 2010F STEM outfitted with a URP pole piece, GATAN 2000 GIF, GATAN DigiScan II, Fischione HAADF STEM detector, Oxford energy-dispersive X-ray detector and EmiSpec EsVision software. STEM images were acquired for fresh and aged samples using the high resolution probe at 2 Å. Electron energy loss spectroscopy (EELS) and EELS spectrum imaging was performed using the 0.2 Å probe, an alpha of 20 mrad, and a beta of 6 mrad.

2.7. Postmortem sulfur analysis

The aged core sample was cut into three 1″ long sections, hereafter denoted as front, middle and rear. The amount of residual sulfur in each section was measured by detecting the SO_2 evolved after heating the ground catalyst sample to 1425 °C using an ELTRA CS 500 Carbon Sulfur Determinator. Powder X-ray diffraction (XRD) measurements were performed on a Phillips X'Pert diffractomer using Cu K_α radiation (λ = 1.5406 Å) and a step size of 0.02°. The chemical state of the residual sulfur in the mid-section of the aged core sample was examined by X-ray photoelectron spectroscopy (XPS). XPS measurements were performed on a Kratos AXIS HSi instrument equipped with a charge neutralizer and Mg Kα X-ray source. Spectra were recorded at normal emission using an analyzer pass energy of 40 eV and an X-ray power of 144 W and were energy referenced to CHx at 285 eV. Peak analysis was performed using Casa-XPS Version 2.1.9 software with all spectra Shirley-background subtracted prior to fitting. S 2p spectra were deconvoluted with components having a symmetric Gaussian–Lorentzian lineshape. Elemental compositions were calculated after correction of peak areas for respective atomic sensitivity factors.

3. Results and discussion

3.1. N_2 physisorption and H_2 chemisorption

Physical data for the aged catalysts are listed in Table 3. The corresponding data for the fresh catalysts are also included here as a reference. Evidently, aging resulted in a decrease in washcoat BET surface area and pore volume, associated with the collapse of some of the smaller pores. This is reflected in an increase in average pore radius after aging. Relative to the ceria-free catalyst 30-0, the ceria-containing catalysts displayed a more pronounced decrease in BET surface area, which can be correlated to the more severe sintering of the CeO_2 (or CeO_2-ZrO_2) phase relative to γ-Al_2O_3 [43]. The apparent loss of washcoat surface area for catalyst 30-100Z was unexpected, given the superior thermal stability of CeO_2-ZrO_2 mixed oxides with respect to CeO_2 [44,45]. Although washcoat adhesion for 30-100Z was noted to be inferior to that of the other catalysts, resulting in possible loss of washcoat during aging, the small loss of OSC noted for 30-100Z after aging (see below) suggests that any washcoat loss was very minor.

According to H_2 chemisorption measurements, aging induced severe sintering of the precious metals (PMs), as evidenced by a significant drop (73–82%) in the overall PM dispersion regardless of whether ceria was present or not. For the fresh catalysts, a higher metal dispersion for the ceria-containing catalysts relative to 30-0 can be attributed to the contribution of highly dispersed Pt supported on the CeO_2 or CeO_2-ZrO_2 phases. However, aging almost eliminated the benefit of CeO_2 addition in improving the PM dispersion. This can be attributed in part to the sintering of the CeO_2 itself, which can be expected to result in some degree of PM encapsulation [46,47].

As outlined above, precious metal sintering has been recognized as a major limitation with respect to the durability of LNT catalysts. It has been reported that PM sintering is dependent on gas composition, temperature and duration, with oxidizing atmospheres resulting in particularly severe Pt sintering [48,49]. To simulate on-road aging, in this study desulfation was performed under lean-rich cycling conditions in order to minimize H_2S formation during rich operation (as typically done for real world applications). During each aging cycle, the catalysts were exposed to two high-temperature events: desulfation at 700 °C (500 min in total for the 50 aging cycles used) and subsequent simulated DPF regeneration at 650 °C under continuous lean conditions (25 h in total). Based on the foregoing, both sets of conditions can be expected to be responsible for PM sintering to some degree.

3.2. Electron microscopy analysis of fresh and aged catalyst samples

3.2.1. 30-0, fresh sample

According to TEM observations, the washcoat morphology of 30-0 in the fresh state consists of nest-like agglomerations of spear-shaped γ-alumina crystals with length scales ranging from ~10 to 35 nm, and corresponding width of ~3 to 10 nm (Fig. 3a). Adjacent to Al_2O_3 are Ba oxide particles with a distinctly denser granular morphology, although some occur as nano-layers coating Al_2O_3 crystals. In STEM imaging mode, Ba-rich areas appear brighter compared with the Al support, indicating that the Ba oxide shows relatively good surface coverage (Fig. 3b). EDS analyses were performed to further distinguish the washcoat components. Pt nanoparticles are dispersed on the surface of both Al_2O_3 and Ba grains, but the density of Pt particle accumulation is greater on the Ba-rich areas as demonstrated in the STEM image in Fig. 3c. The Pt particles on Al_2O_3 surfaces display a narrow size range with the

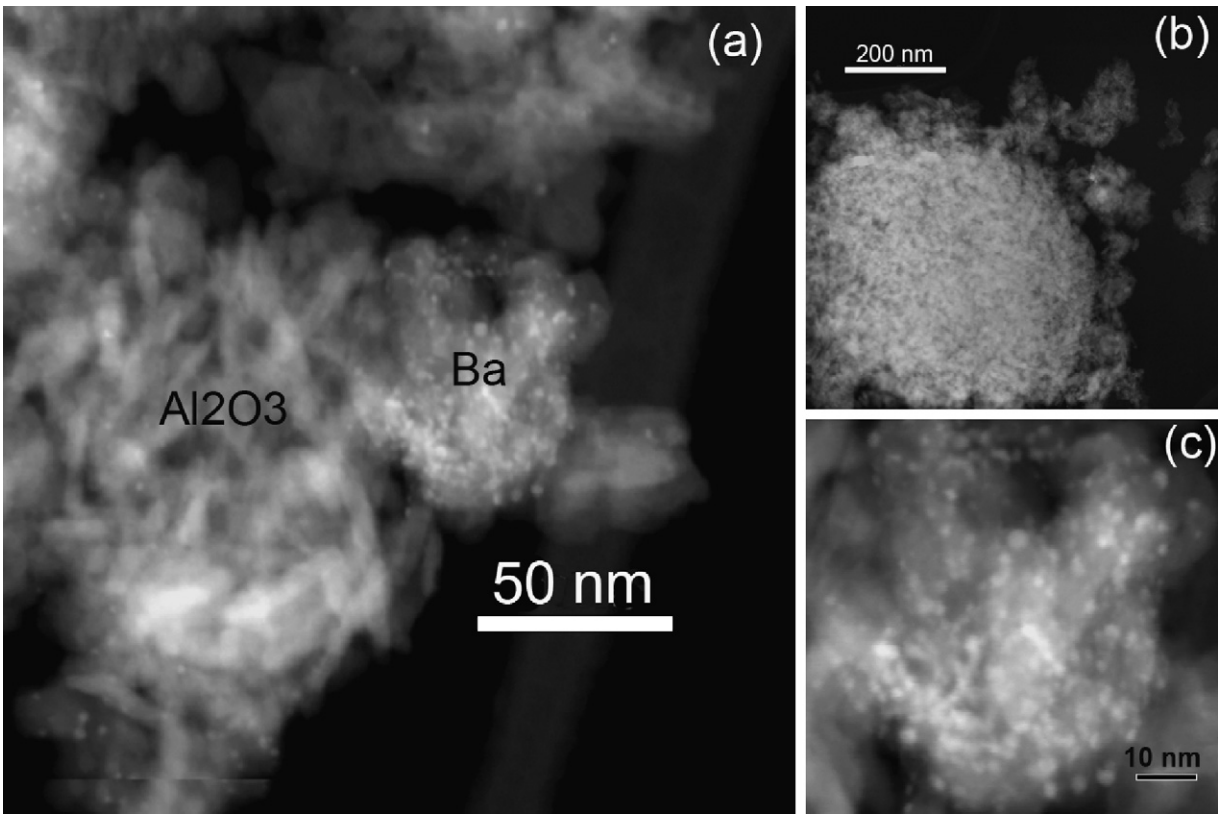

Fig. 3. STEM images for fresh 30-0 illustrating (a) Al_2O_3 support and Ba regions with small Pt nanoparticles at the surfaces, (b) Ba-rich areas with Al_2O_3 support, and (c) Ba agglomerate with Pt (white areas).

majority of particles ~2 nm in size while Pt on Ba-rich surfaces show a broader size range from 1 to 4 nm.

3.2.2. 30-0, aged sample

The aged sample has a markedly denser surface appearance compared with the fresh material and the STEM image (Fig. 4a) illustrates the presence of rather large Pt crystals, some as big as 25 nm that have accumulated on the washcoat surface. The spear-shaped Al_2O_3 crystals host only minor amounts of Pt particles that are still in the original 2 nm size range. The majority of Pt occurs within regions that are coated by a $BaSO_4$ phase which has no morphologically unique characteristics other than showing different layer thickness on various washcoat grains (Fig. 4b). The EDS spectrum in Fig. 4c shows the presence of both Ba and S in the region with high Pt particle density; Pt particles in this region demonstrate a wide size range from 2 to 25 nm. There is evidence that Pt particle growth occurred due to migration and coalescence as evidenced in Fig. 4a, where Pt particles are shown that clearly have fused together. When compared with the fresh washcoat morphology, the $BaSO_4$ phase seems more evenly coated on the Al_2O_3 compared with the BaO in fresh 30-0, suggesting that some Ba was mobilized prior to formation of $BaSO_4$.

3.2.3. 30-100, fresh sample

The alumina support consists of agglomerates made up of networks of elongated Al_2O_3 crystals as in sample 30-0, with locally enriched zones consisting of CeO_2. The presence of ceria-rich areas can be optically distinguished from the alumina support in the STEM image in Fig. 5a, since STEM mode depicts heavier elements with a brighter reflection. Adjacent to and on top of the Al_2O_3 are granular Ba deposits (Fig. 5b), which was confirmed using both EDS and EELS. Fig. 5c indicates that Pt nanoparticles on both Ba and Al surfaces have a narrow size range from 2 to 6 nm. The Pt catalyst particles hosted on ceria surfaces (the presence of which was confirmed by EELS) are noticeably smaller, ranging from 1 to 2.5 nm (Fig. 5d).

3.2.4. 30-100, aged sample

After aging, the washcoat in sample 30-100 contains large (up to 30 nm) Pt particles, although the majority of Pt particles are in a size range from 3 to 15 nm. Platinum grains appear to have significantly grown due to sintering or coalescence (similar to those in aged sample 30-0). Pt particles on CeO_2 have grown to a size of up to 5 nm, suggesting significantly less sintering of Pt on the ceria support in contrast to Al_2O_3 surfaces, while the ceria support clearly has a less well defined nanocrystalline morphology after aging. The latter observation is indicative of densification of the ceria phase; this is consistent with sintering of the ceria, although it should not be regarded as conclusive. There are also dense sulfur-rich Ba nodules present on the Al_2O_3 surface (Fig. 6a). The EDS spot analysis in Fig. 6b was performed at the area marked in Fig. 6a and identified Ba, S, Al and Pt, pointing toward the fact that the $BaSO_4$ nodules were present on the surface of the Al_2O_3 support. The EELS spectrum taken over the entire sulfur-rich nodule clearly shows two sharp peaks for Ce M_5 M_4 and also for Ba M_5 M_4 (Fig. 6c), as well as signals for O and Al (note that the signal for Al appears outside of the energy range depicted in Fig. 6c). This suggests that the beam penetrated the ceria particles and also probed underlying BaO/Al_2O_3 particles. The presence of sulfur was not confirmed as a typical surface coating on top of ceria-rich areas, but occurred immediately at the exterior of ceria grains together with Al and Ba. This was confirmed using an EELS trace line scan, as shown in Fig. 6. The trace line analyzed multiple EELS spectra along a distance that spanned from the alumina support across the ceria-rich area. The objective was to look for any significant sulfur enrichment along the line, particularly in the immediate vicinity of

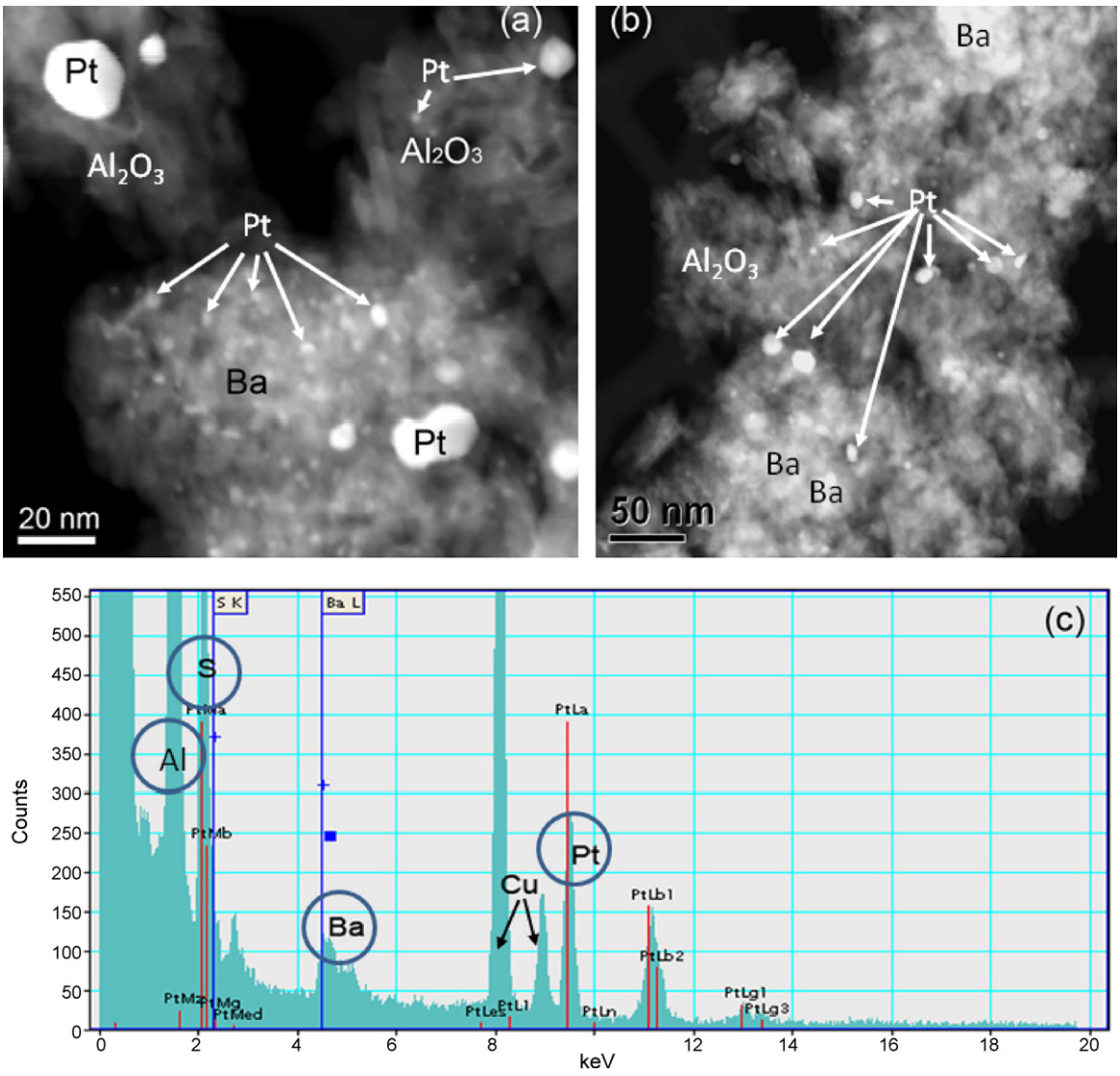

Fig. 4. STEM images for aged 30-0 (a and b) illustrating large particle size range for Pt shown in white; (c) EDS spectrum.

CeO_2. The EELS line scan results indicate that S is clearly enriched at the interface of the CeO_2 and Al_2O_3 support, but does not occur where only ceria is located. Furthermore, sulfur is only observed in the presence of Ba.

3.3. Residual sulfur analysis

The residual sulfur concentrations in the three different sections of the aged catalysts are reported in Fig. 7. Sulfur contents in the three sections of each catalyst are rather similar, although there is a tendency for slightly higher sulfur accumulation in the rear of the catalysts. The overall residual sulfur content in the washcoat is in the range 0.8–1.1 wt%. Assuming that all of the sulfur was adsorbed during sulfation, around 95% of the adsorbed sulfur was removed during desulfation (including the final desulfation step at 750 °C). At first sight, catalyst composition does not appear to influence the residual sulfur loading. However, if the sulfur content is normalized to the actual Ba loading (given that the measured Ba loading varied slightly from sample to sample), it is apparent that the S/Ba ratio tends to decrease with increasing ceria loading (albeit that there are only three data points; see Fig. 7). This finding suggests that the presence of ceria can inhibit the sulfur poisoning of the Ba phase, consistent with our previous findings for model powder catalysts [36].

XPS analysis was used to examine the oxidation state of the sulfur in the aged catalysts. The S 2p lines for sulfate, sulfite and sulfide are located at around 170 eV (sulfate), 167 eV (sulfite) and 162 eV (sulfide). Only sulfate was observed in aged samples 30-0 and 30-100, as evidenced by the S 2p line located at ~170 eV (Fig. 8). The fact that no sulfide was present in the aged samples can be ascribed to two reasons: the involvement of both H_2O and CO_2 in the desulfation process [12,50,51] and the use of the cycling mode for desulfation [52]. Aluminum and cerium sulfates can be reductively decomposed at lower temperatures than $BaSO_4$ (below 600 °C) [7,37], implying that the residual sulfur phase is Ba sulfate (given that a desulfation temperature of 700 °C was applied during aging). This could not be confirmed by X-ray diffraction due to the low concentrations involved, although as discussed above, TEM data clearly show that sulfur present in aged 30-0 and 30-100 is associated with barium. For other catalysts containing higher concentrations of Ba, e.g., corresponding to a BaO loading of 45 g/L, it did prove possible to establish the presence of crystalline $BaSO_4$ by XRD; these results will be presented in a separate paper [53]. It should be noted that in no cases was the presence of $BaAl_2O_4$

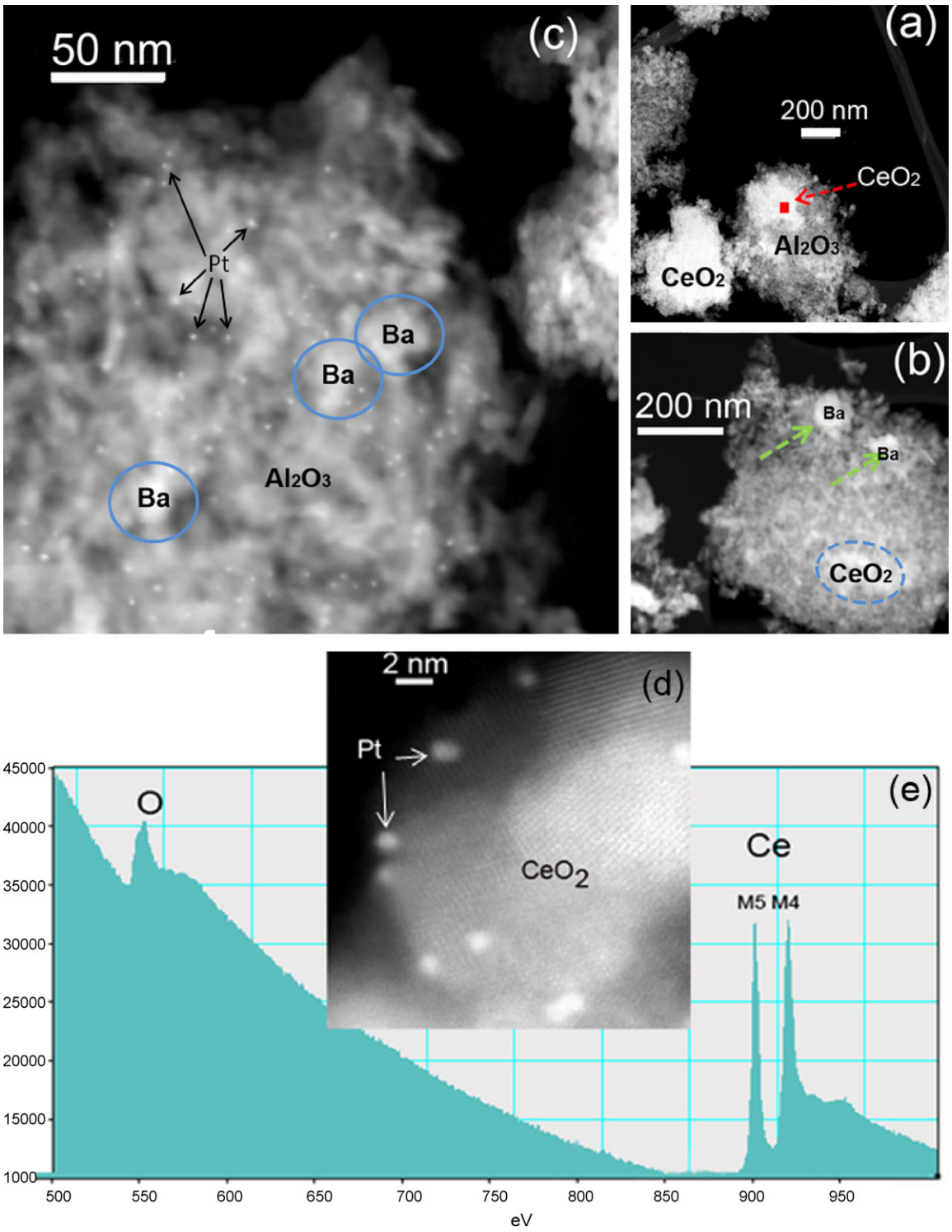

Fig. 5. STEM images for fresh 30-100 showing (a) Al_2O_3 support with adjacent CeO_2 (bright zones), (b) Al_2O_3 support with granular Ba-rich nodules, (c) Al_2O_3 support with locally enriched Ba and Pt nanoparticles, (d) highly crystalline nanosized ceria crystals host ultra-small Pt nanoparticles, (e) EELS analysis: ceria.

observed, consistent with the fact that the maximum temperature to which the catalysts were exposed during aging did not exceed ~780 °C.

Comparing the S/Ba mole ratios determined by elemental analysis with the S/Ba ratios obtained from XPS analysis (Fig. 7), it is apparent that for both 30-0 and 30-100 there is a slight difference between the two, indicating that sulfur was not distributed uniformly throughout the bulk of Ba phase but was instead somewhat concentrated at the surface and sub-surface sites detected by XPS.

3.4. Oxygen storage capacity

The oxygen storage capacity (OSC) of the aged catalysts was determined under conditions used previously for the measurement of OSC in the fresh catalysts [38]. The H_2 concentration

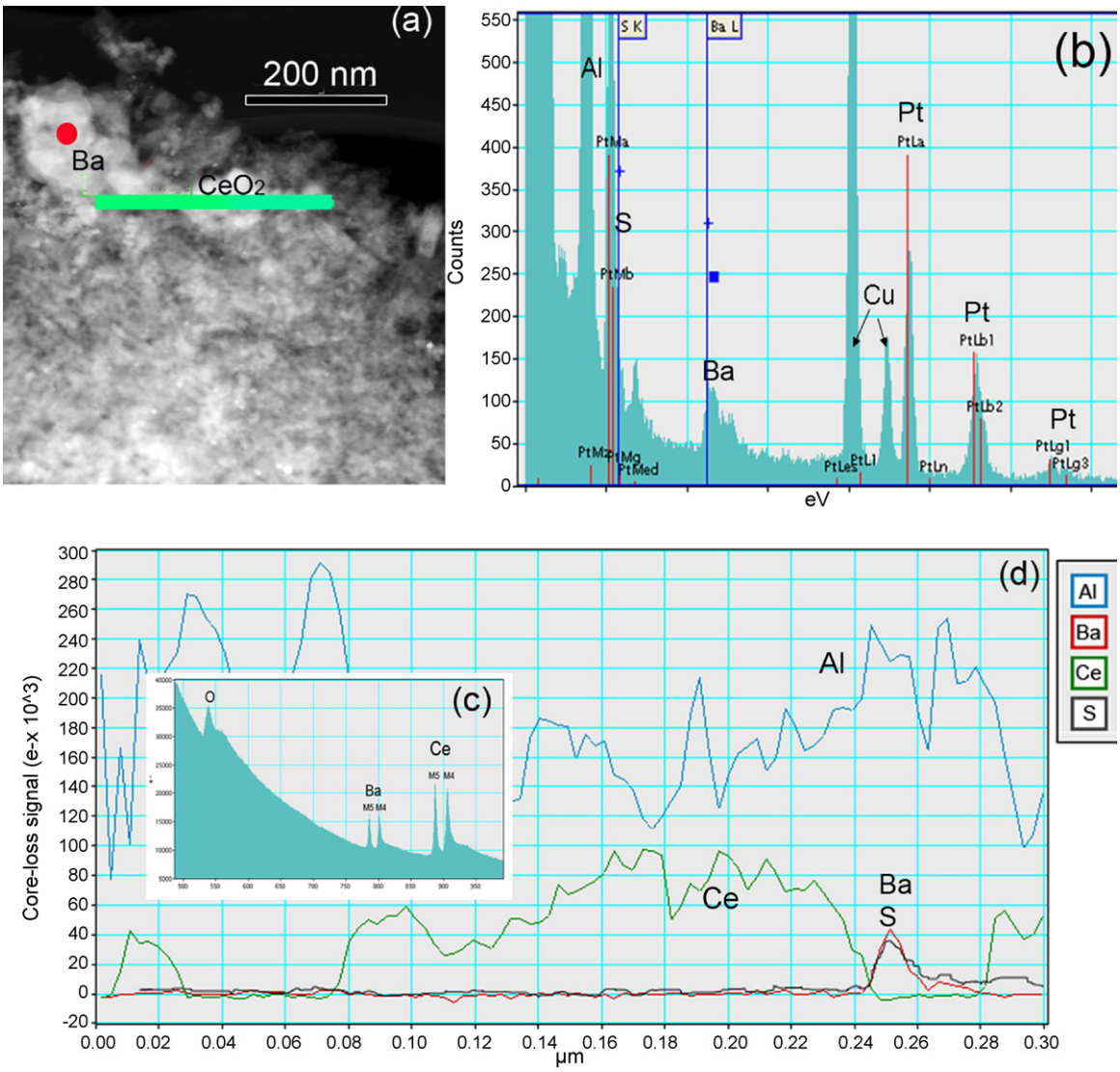

Fig. 6. (a) STEM image for aged 30-100 showing Al_2O_3 support and Ba-rich nodules, as well as a CeO_2-rich area. The solid line indicates the EELS line scan region; (b) EDS spectrum recorded at the marked dotted area shown in (a); (c) EELS spectrum taken at the dotted area in (a); (d) EELS trace-line: the line is shown in (a). The trace line included 50 EELS measurements along the distance. S-enrichment is seen at the interface between Al_2O_3 and CeO_2.

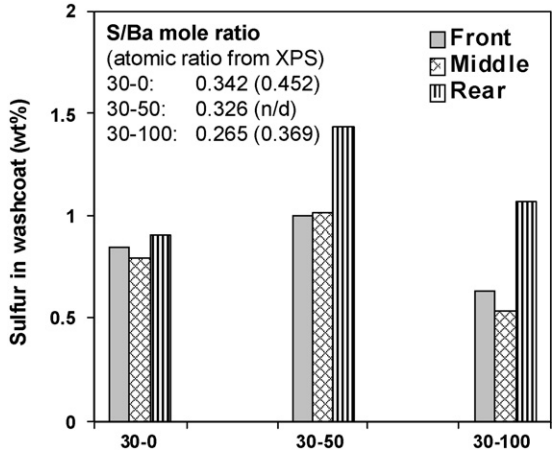

Fig. 7. Residual sulfur content in aged catalysts after reduction at 750 °C for 10 min. S/Ba ratios determined from elemental analysis refer to the whole catalyst; ratios determined from XPS data refer to the middle sections of the catalysts.

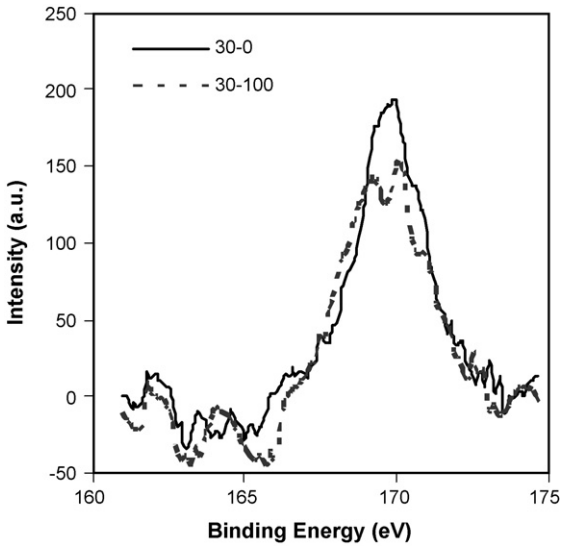

Fig. 8. Sulfur 2p X-ray photoelectron spectra of aged 30-0 and 30-100.

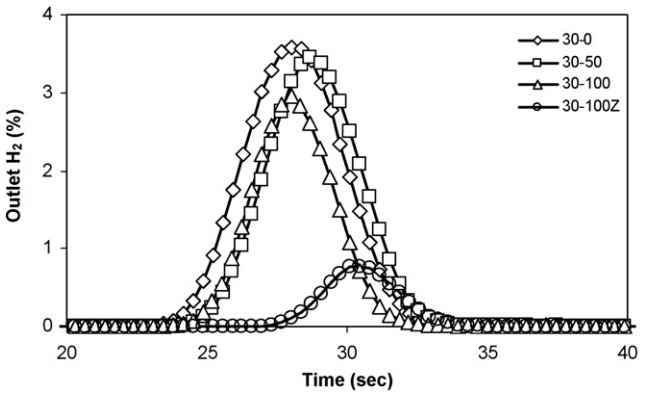

Fig. 9. Outlet H_2 concentration profiles for the aged samples during oxygen storage measurement under cycling conditions at 350 °C (inlet H_2 concentration = 4.2%).

profiles at the catalyst outlet are shown in Fig. 9. In all cases, the catalysts exhibited shorter breakthrough times after aging, consistent with decreased OSC. While the difference in breakthrough times between aged 30-0 and the aged La-stabilized ceria-containing catalysts was relatively small, a much longer breakthrough time, along with a much smaller peak H_2 concentration, was observed for the aged 30-100Z (containing CeO_2-ZrO_2), indicative of greatly increased H_2 consumption by stored oxygen in this catalyst relative to the others. From the calculated oxygen storage capacities (Table 4), it was found that while 30-0 showed only a small decrease in OSC (<10%) after aging, the drop in OSC for aged 30-50 and 30-100 amounted to ~30%. Of the four aged catalysts, aged 30-100Z showed the highest residual OSC, the measured value of 69.6 mmol/L representing 95% of the OSC value measured for the fresh catalyst. This small loss in OSC for aged 30-100Z compared to aged 30-100 can be ascribed to the fact that whereas OSC in CeO_2 is associated principally with the oxide surface (and hence can be expected to show a strong dependence on surface area), in CeO_2-ZrO_2 bulk oxygen storage plays a dominant role [45]; hence the OSC of CeO_2-ZrO_2 after aging is not expected to be as sensitive to the loss of surface area.

Table 4
Comparison of OSC and NO_x reduction selectivity to N_2 and NH_3 under lean-rich cycling at 350 °C.

Catalyst	OSC (mmol/L)		N_2 selectivity (%)		NH_3 selectivity (%)	
	Fresh	Aged	Fresh	Aged	Fresh	Aged
30-0	21.5	19.4	66.4	22.8	30.7	75.8
30-50	38.1	26.0	89.6	69.2	9.3	29.2
30-100	55.9	39.7	95.8	87.2	2.1	10.6
30-100Z	73.2	69.5	97.0	88.1	1.8	9.7

3.5. NO_x storage

The NO_x storage and regeneration behavior of the aged catalysts was investigated on a bench reactor. Concentration profiles

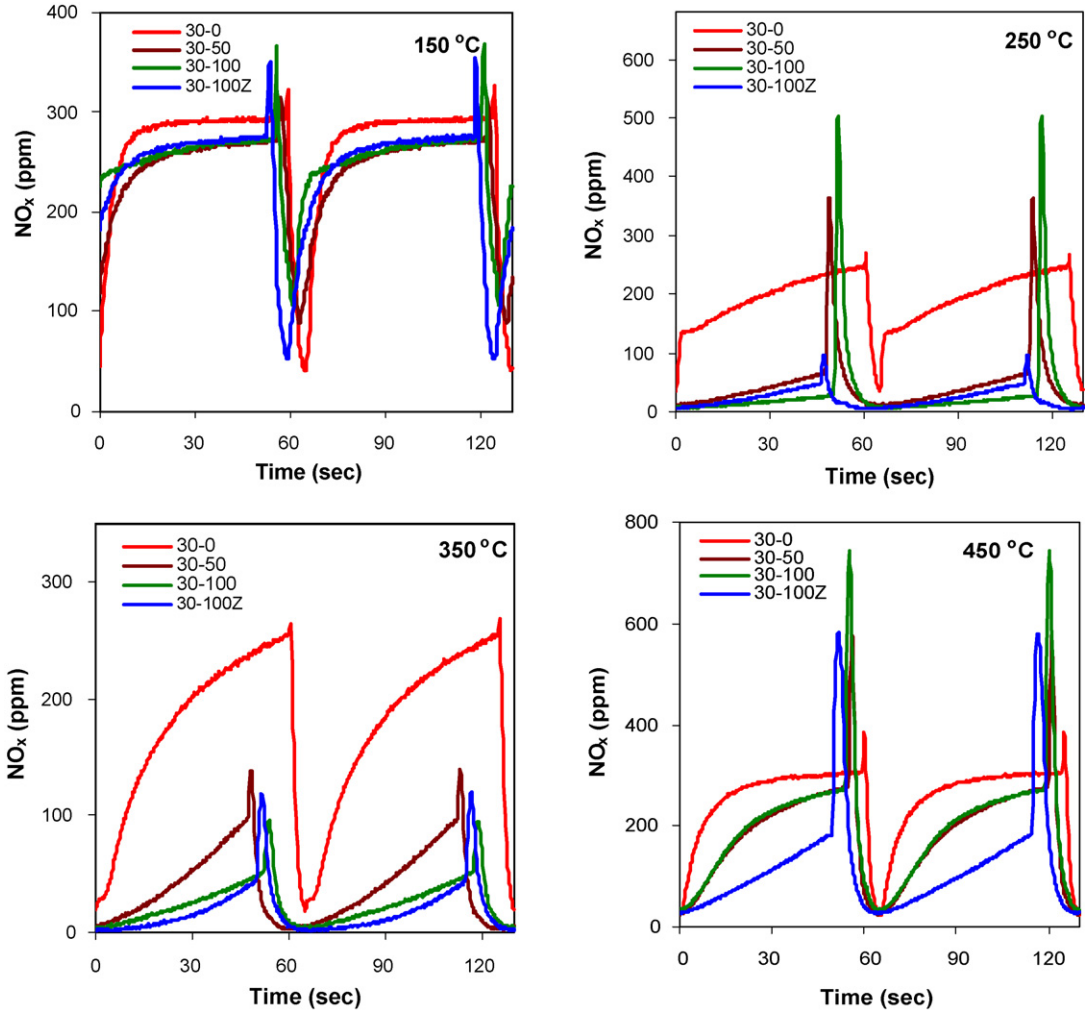

Fig. 10. NO_x slip during lean-rich cycling at different temperatures for aged catalysts. Note that for clarity, the NO_x profiles have been staggered.

Table 5
Comparison of NO_x storage and release during lean-rich cycling.

Catalyst	Temperature (°C)	Lean-phase NO_2 slip (μmol)[a]		Lean-phase NO_x storage efficiency (%)		Rich-phase NO_x release (%)[b]		Cycle-averaged NO_x conversion (%)	
		Fresh	Aged	Fresh	Aged	Fresh	Aged	Fresh	Aged
30-0	150	61.3	50.7	20.3	14.6	31.2	35.5	14.0	9.4
	250	5.4	103.1	94.7	38.0	0.7	9.5	94.1	34.3
	350	1.6	74.5	96.8	43.2	1.0	7.4	95.9	40.0
	450	9.8	52.9	76.1	17.4	11.6	25.7	67.3	12.9
30-50	150	52.5	47.6	35.2	21.2	27.7	28.3	25.5	15.2
	250	0.4	14.3	99.7	89.1	0.1	6.3	99.6	83.5
	350	0.1	14.2	99.8	88.7	0.0	2.3	99.8	86.7
	450	4.5	35.3	94.2	44.3	9.2	17.6	85.5	36.5
30-100	150	17.8	54.3	56.5	17.9	37.3	36.5	35.4	11.4
	250	0.0	6.3	98.8	94.5	0.1	7.1	98.6	87.7
	350	0.1	8.4	99.6	92.8	0.1	1.8	99.6	91.1
	450	6.5	34.7	82.4	41.9	24.0	28.9	62.6	29.8
30-100Z	150	25.5	39.5	30.1	20.8	27.7	26.7	21.8	15.3
	250	1.2	9.4	97.0	93.4	0.5	1.4	96.5	92.0
	350	0.8	4.8	97.7	95.5	0.3	2.3	97.4	93.3
	450	0.0	17.3	75.7	69.7	10.5	17.0	67.7	57.8

[a] The total amount of input NO per lean-rich cycle was 171.5 μmol.
[b] (NO_x released in rich purge/NO_x stored in lean phase) × 100%.

pertaining to NO_x storage and release under steady state cycling conditions are shown in Fig. 10 and a summary of the measured NO_x storage is given in Table 5. Note that here, and throughout the following text, "NO_x release" refers to that portion of the NO_x, formed from decomposition of the nitrates/nitrites, which is not reduced in the catalyst (i.e., the rich phase NO_x slip). Similar to the fresh catalysts [38], each of the aged catalysts showed higher lean phase NO_x slip at 150 and 450 °C relative to 250 and 350 °C. Furthermore, the ceria-free catalyst showed significantly higher lean phase NO_x slip than the ceria-containing samples at the four temperatures investigated, reflecting its more rapid saturation with NO_x. For each of the aged catalysts NO_2 was observed during the lean phase of the cycling (Table 5), indicating that NO_x storage capacity was not limited by the kinetics of NO oxidation for the aged catalysts. Compared to the fresh catalysts, in nearly all cases the lean phase NO_2 slip increased after aging, with the ceria-free catalyst 30-0 showing much higher NO_2 slip than the other samples.

Examination of the lean phase NO_x storage efficiency (NSE) calculated from the lean-rich cycling data reveals that aging caused a decrease in NSE for all the catalysts in the range 150–450 °C. Relative to the ceria-containing catalysts, 30-0 showed a significant drop in NSE in the range 250–350 °C, with only ~40% of the inlet NO_x being stored during the lean phase after aging. In contrast, a NSE of above 90% was still achieved for the aged 30-100, while that for aged 30-100Z was ~95%. Evidently, the addition of ceria (and ceria–zirconia) significantly reduced the impact of aging on the NO_x storage capacity.

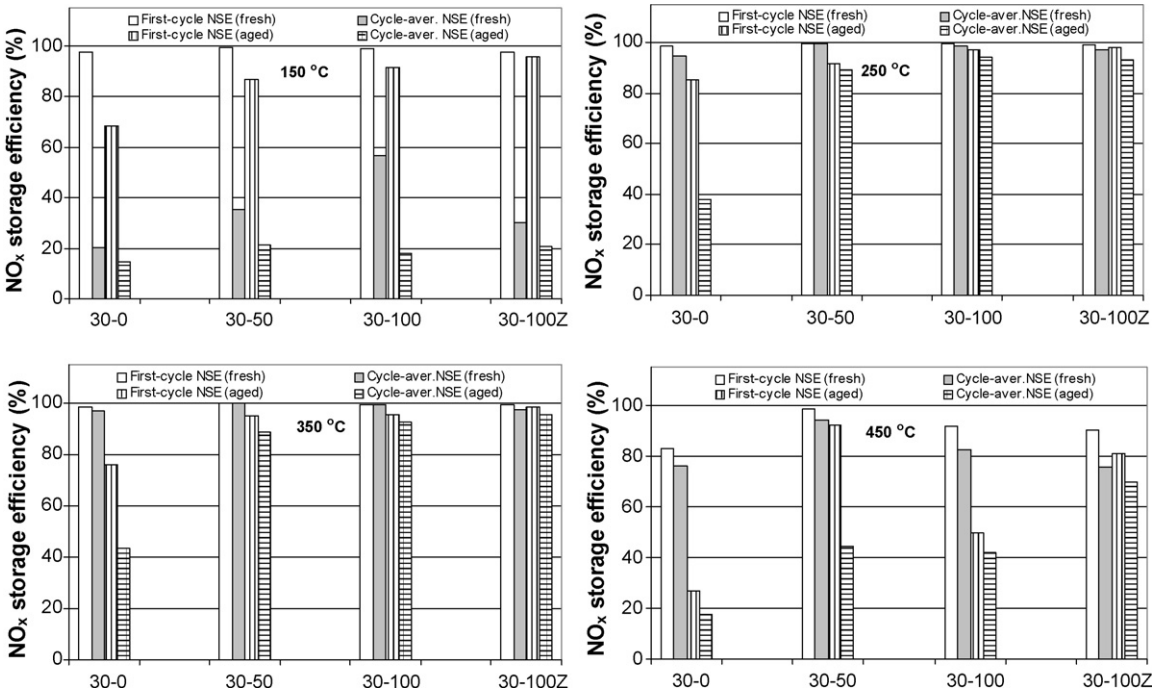

Fig. 11. Comparison of NO_x storage efficiency during the first cycle and during lean-rich cycling for fresh and aged catalysts.

To understand the origin of the decreased NSE after aging, it is insightful to compare the NSE measured during the lean phase of the first cycle after complete catalyst regeneration at 500 °C—representing the "intrinsic" or maximum NSE (i.e., the NSE for a catalyst initially totally free of NO_x)—with the NSE measured under steady state cycling (i.e., cycling conditions under which the periodic behavior of the catalyst is constant from one cycle to the next). It must be appreciated that during cycling, the catalyst is not completely regenerated (unless the rich phase is extremely long and/or the temperature very high, which was not the case here). Hence, the NSE measured under cycling represents the product of the intrinsic NSE and the extent to which the NO_x storage sites are regenerated by rich purging during lean-rich cycling. As shown in Fig. 11, only slight differences in the intrinsic NSE were observed between the fresh catalysts. Indeed, the intrinsic NSE value reached a value of ~99% in the range 250–350 °C for each of the fresh catalysts, while only a slight drop in the NSE was observed during subsequent cycling. Evidently, the fresh catalysts are able to maintain a good balance between NO_x storage and regeneration.

Turning to the aged catalysts, the main trends observed are best illustrated by consideration of the data collected at 350 °C (Fig. 11). A drop in the first cycle NSE was observed for each of the catalysts after aging, reflecting a decrease in their intrinsic capacity for NO_x storage. This was most apparent for 30-0, which showed an absolute decrease of 22% in first cycle NSE, compared to relatively minor decreases of 4% for 30-100 and 2% for 30-100Z. If the first cycle NSE values are then compared with the cycle-averaged NSE values for the aged catalysts, it is apparent that in the case of catalyst 30-0 a significant discrepancy exists. More specifically, the cycle-averaged NSE value of 43% versus 76% for the first cycle NSE, indicates that the NO_x storage efficiency of the aged 30-0 was significantly limited by its inability to be completely regenerated during rich purging. In contrast, the small differences observed between the first cycle and cycle-averaged NSE values for 30-100 and 30-100Z (3% in both cases) indicate that these two catalysts retained their good regeneration characteristics. The presence of ceria (or ceria–zirconia) was thus highly beneficial to not only the intrinsic NSE but also the regeneration efficiency after aging.

At 150 and 450 °C poor cycle-averaged NSE was responsible for significant declines in overall NO_x conversion for all of the catalysts. As shown in Fig. 11, for catalysts 30-0, 30-100 and 30-100Z, the observed decrease in cycle-averaged NSE at 450 °C is explained almost wholly by the loss of first cycle NSE at this temperature (although 30-50, for reasons that are not apparent, does not follow this trend). Given that ceria and ceria–zirconia do not significantly contribute to NO_x storage at 450 °C [54,55], this loss of intrinsic NSE can be attributed to degradation of the NO_x trapping ability of the Ba phase. In contrast, NO_x storage at 150 °C can be expected to occur to a large extent on the CeO_2(-ZrO_2) phase [38]. From the data in Fig. 11, it is apparent that the first cycle NSE for 30-50, 30-100 and 30-100Z at 150 °C is only slightly deteriorated after aging. Hence, the decrease in cycle-averaged NSE at this temperature can be largely attributed to deterioration in the ability of the catalysts to be regenerated during rich purging.

These results clearly show that decreases in cycle-averaged NSE after aging can be attributed to a combination of two factors, namely, decreased intrinsic NSE, and a decrease in the efficiency of catalyst regeneration during rich purging. Furthermore, the relative importance of these two factors depends on the catalyst composition and the temperature of operation. Several explanations can be advanced to account for the decreased intrinsic NSE after aging, including (i) changes in the Ba phase, such as agglomeration of the $BaCO_3$ particles, or the formation of $BaAl_2O_4$, although no evidence for either of these occurrences could be found based on powder X-ray diffraction analysis (data not shown), and (ii) incomplete desulfation of the main Ba NO_x storage phase (i.e., some proportion of the Ba sites were still poisoned by sulfur). While both explanations would lead to a reduction in the number of Ba sites available for NO_x storage, analytical data support the latter explanation. From the S:Ba atomic ratio determined by XPS, and assuming that all of the residual sulfur is associated with the Ba phase, approximately 45% of the surface Ba sites for aged 30-0 are occupied by residual sulfur, while the figure for 30-100 amounts to 37%.

In the case of the deterioration in regeneration efficiency after aging, which together with the decreased intrinsic NSE contributes to the decrease in NSE during lean-rich cycling, PM sintering can be singled out as the probable cause. As reported in the literature, Pt sintering can actually improve NO oxidation activity, given that the turnover frequency for NO oxidation increases with Pt particle size [56,57]. In contrast, decreased NO_x reduction activity is typically associated with PM sintering, as reported in the literature for three-way catalysts [58]. It is generally accepted that the reductant (in this case, H_2 and/or CO) needs to be first adsorbed on the PM before NO_x reduction can occur. Given that sintering results in decreased PM surface area and hence a decrease in available sites for NO_x dissociation and reductant adsorption, the intrinsic rate of NO_x reduction (i.e., the chemical kinetics) is expected to decrease. At the same time, PM sintering also lessens the contact between the Ba and PM phases in LNT catalysts. Indeed, segregation of the Ba and Pt can be partially responsible for the decrease in intrinsic NSE after aging due to the less efficient NO_x transport (spillover) from Pt to Ba that can be expected during NO_x adsorption. It is also likely that the decreased contact between the PM and Ba phases after aging can significantly influence nitrate decomposition and NO_x reduction behavior; a decrease in the rate of reductant spillover from Pt to Ba would decrease the extent of nitrate decomposition during rich purging, while a decrease in the rate of reverse NO_x spillover (Ba to Pt and Rh) could adversely affect the overall rate (and hence efficiency) of NO_x reduction. Indeed, a recent study by Clayton et al. [59] has shown that LNT regeneration activity decreases with decreasing Pt dispersion (see discussion in Section 3.6 below), although it remains to be elucidated which of these processes (reductant transport, NO_x transport, NO_x reduction) is rate determining for the overall kinetics of LNT regeneration.

Turning to the role of ceria (and ceria–zirconia) in ameliorating the effects of aging on catalyst performance, there are several factors which may account for the high cycle-averaged NSE values observed for the aged catalysts 30-50, 30-100 and 30-100Z relative to 30-0. First, ceria can be directly involved in NO_x storage/reduction as a supplement to the main NO_x storage component (Ba); using in situ DRIFTS and reactor studies, we [54,60] and others [61] have shown that the NO_x storage capacity of ceria is appreciable at temperatures below 400 °C. Hence, even if the NO_x storage capacity of the Pt/Ba/Al_2O_3 component is degraded as a result of aging, NO_x storage can still proceed on the Pt/CeO_2(-ZrO_2) component. Similarly, the Pt/CeO_2(-ZrO_2) component can contribute to NO_x reduction. Indeed, studies using both monolithic and powder model catalysts in the fresh state have shown that addition of Pt/CeO_2 to Ba-based LNTs results in improved regeneration characteristics [38,60]. Furthermore, unlike the Pt/Ba/Al_2O_3 component, for which segregation of the Pt and Ba phases can occur during aging, migration and sintering of Pt in the Pt/CeO_2(-ZrO_2) component cannot lead to segregation, i.e., the Pt and CeO_2(-ZrO_2) remain in intimate contact, which should be beneficial for the retention of NO_x storage efficiency, as well as NO_x release (which is generally believed to be initiated by spillover of reductants from the Pt sites to the storage material [62]) and subsequent NO_x reduction. Obviously, this benefit is confined to the Pt/CeO_2(-ZrO_2) component, given that significant reductant spillover from Pt/CeO_2(-ZrO_2) to Pt/Ba/Al_2O_3 is unlikely owing to

the two components being present in the washcoat as a physical mixture. For the $Pt/CeO_2(\text{-}ZrO_2)$ component, sintering of the support (as reflected in the decrease in OSC and washcoat surface area) is indicated to be an important aging mechanism, as this can result in some degree of Pt encapsulation [46,47]. Sintering of the Pt itself is also indicated by TEM data (as discussed in Section 3.2), although the ceria-supported Pt particles imaged in aged 30-100 were significantly smaller than those associated with the Al_2O_3 or BaO phases. These observations are in agreement with previous studies indicating that ceria is a good support for stabilizing high dispersions of Pt due to the strong $Pt–CeO_2$ interaction [63]. Indeed, in a recent study [64], it was found that thermal aging of Pt supported on Ce-Zr-Y mixed oxide at 800 °C in air did not result in measurable Pt sintering according to CO chemisorption data. EXAFS data were consistent with a strong interaction between the Pt and the support, as indicated by the presence of Pt–O–Ce bonding. It is worth noting that the EXAFS data also showed that this bond is broken upon reductive treatments; hence, when ceria is used as a support, Pt sintering is likely to occur via particle migration and coalescence under reducing conditions.

Second, ceria-containing catalysts exhibit superior sulfation and desulfation characteristics as compared to their non-ceria analogs. Using the same catalysts employed in this study, we have shown that relative to 30-0 (containing no ceria), catalysts 30-50, 30-100 and 30-100Z display a greater resistance to deactivation during sulfation (as reflected by cycle-averaged NSE values), and require lower temperatures to restore the NO_x storage efficiency to its pre-sulfation value [37]. Additionally, the $CeO_2(\text{-}ZrO_2)$ containing catalysts release greater fractions of stored sulfur during desulfation. These findings reflect the ability of ceria to store sulfur and release it at relatively low temperatures under reducing conditions. As a result, when ceria is present the Ba phase is to some degree protected from sulfation, as shown in a recent DRIFTS study [36]. In the context of catalyst aging, these findings have two main consequences. First, when subjected to repeated sulfation–desulfation cycles, the ceria-containing catalysts should accumulate less sulfur on the Ba phase than 30-0. A comparison of the XPS data for 30-0 and 30-100 appears to confirm this, while the elemental analysis data shown in Fig. 7 also show a clear trend with respect to the S:Ba mole ratio. Second, as indicated above, after sulfation, catalysts 30-50, 30-100 and 30-100Z display superior NO_x storage and reduction properties to 30-0 subjected to the same degree of sulfation [37]. While this may indeed be a consequence of lessened sulfur accumulation on the Ba phase, the ability of the $Pt/CeO_2(\text{-}ZrO_2)$ component to contribute to NO_x storage and reduction should also be of importance.

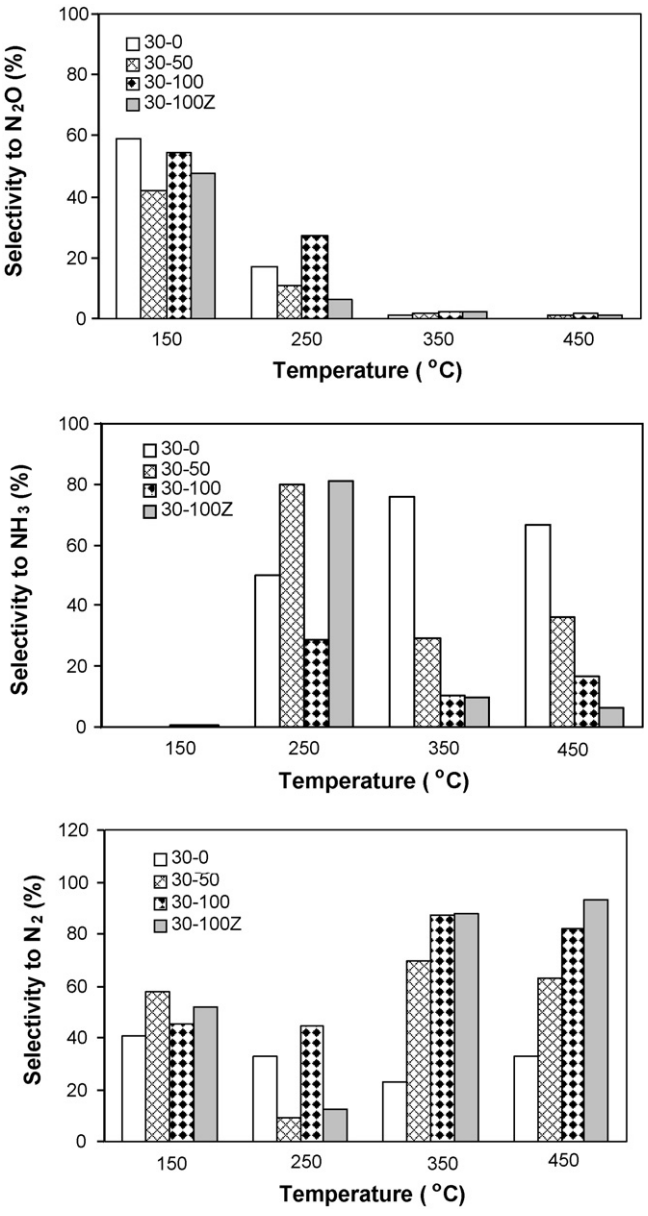

Fig. 12. Selectivity to N_2O (top), NH_3 (middle) and N_2 (bottom) for NO_x reduction during lean-rich cycling.

3.6. NO_x release and reduction

As shown in Table 5, the aged ceria-containing catalysts displayed both lower lean phase NO_x slip and lower rich phase NO_x release than 30-0 (by integration of the NO_x signals), albeit that peak NO_x concentrations measured at the reactor outlet during rich purging sometimes exceeded those of 30-0 (Fig. 10). For example, in the case of 30-100, peak rich phase NO_x concentrations reached ~500 ppm at 250 °C and 700 ppm at 450 °C. The observation of such high, transient NO_x concentrations during rich purging points toward an imbalance between the rates of nitrate decomposition and NO_x reduction, particularly in the case of 30-100 and 30-100Z. As shown in Table 5, all of the catalysts showed an increase in the percentage rich phase NO_x release after aging, i.e., an increase in the amount of NO_x released as a percentage of the NO_x stored during the lean phase. This reflects a deterioration in the NO_x reduction function of the catalysts caused by aging. Similar to the fresh catalysts, the aged catalysts showed the lowest NO_x release percentage in the range 250–350 °C, where the best performance is achieved for all of them. As shown in Table 5, the cycle-averaged NO_x conversion in the range 250–350 °C follows the order: 30-100Z > 30-100 > 30-50 > 30-0. At 350 °C, for example, 30-100 and 30-100Z achieved a NO_x conversion of 91% and 93% respectively, versus 40% for 30-0. This large discrepancy follows from the fact that the $CeO_2(\text{-}ZrO_2)$ containing catalysts displayed both superior cycle-averaged NO_x storage and NO_x reduction properties than 30-0.

The product selectivity of the catalysts with respect to NO_x reduction during rich purging is shown in Fig. 12. As we have reported previously for the fresh catalysts, N_2O is the dominant NO_x reduction product at low temperature (150 °C). NH_3 is mainly formed at ~250 °C and N_2 becomes the major product at high temperature (350 and 450 °C). Different from N_2O, the formation of N_2 and NH_3 were significantly impacted by the addition of ceria in the temperature range 250–450 °C, the presence of ceria resulting in improved selectivity to N_2. However, as shown in Table 4,

compared to the fresh catalysts, all of the catalysts showed lower N_2 selectivity and higher NH_3 selectivity in the range 250–450 °C after aging. Recent studies have shown that the product distribution during NO_x reduction is a function of the relative NO_x and reductant concentrations, i.e., high H_2:NO_x ratios favor the formation of NH_3 [65]. Since the same amount of reductant was available during rich purging for the fresh and aged catalysts, a higher ratio of reductant to stored NO_x for the aged catalysts (due to the lowered NSE) should result in increased selectivity to NH_3 over N_2.

Although the foregoing is an attractive explanation, it must be stressed that there are several other factors which can affect the selectivity of NO_x reduction. Noteworthy in this regard are the results of an elegant study conducted by Clayton et al. [59]. For model LNT catalysts with different Pt dispersions, it was found that LNT selectivity to NH_3 increased with increasing average Pt particle size. This finding was rationalized on the basis that as the Pt/Ba interfacial perimeter decreases (with decreasing Pt dispersion), the rate of transport of stored NO_x to Pt ("reverse spillover") is decreased. If this rate is slower than the H_2 feed rate, then H_2 will break through with substantially more NO_x remaining on the catalyst after H_2 breakthrough. Consequently, the Pt surface will be predominantly covered by hydrogen, and as the stored NO_x transports to the Pt particles, NH_3 will be preferentially formed. It should be noted that consistent with our results for the fresh versus aged catalysts, Clayton et al. also found that, during lean-rich cycling, the amount of stored NO_x increased with increasing Pt dispersion in the temperature range studied (125–340 °C); this was similarly attributed to the enhanced NO_x spillover from Pt to the Ba phase that should result from the larger Pt surface area and Pt/Ba interfacial perimeter. Likewise, a tendency for slower catalyst regeneration with increasing Pt particle size was also noted, suggesting that a kinetic process, such as reverse spillover of stored NO_x or the spillover of reductant from Pt to the NO_x storage phase may limit the overall rate.

Another factor that can influence the NO_x reduction selectivity of the aged catalysts is their OSC. From Table 4, a comparison between OSC and the selectivity of NO_x reduction reveals that selectivity to N_2 increases with increasing OSC for both the fresh and aged catalysts. As discussed in our previous study [38], there are several possible reasons for this. First, an increase in stored oxygen should result in a decreased reductant concentration in the gas front during rich purging (due to consumption of the reductant by reaction with the oxygen), thereby favoring the formation of N_2 over NH_3. Second, NH_3 formed at the front of the catalyst can be converted to N_2 via reaction with the oxygen stored in the rear of the catalyst. As catalyst OSC is increased, more NH_3 tends to be converted to N_2 at the rear of the catalyst. From Table 4 it is apparent that after aging, all of the catalysts showed decreased selectivity to N_2 during NO_x reduction, the selectivity to NH_3 being increased. Given the apparent dependence of selectivity to N_2 on OSC, and that all of the catalysts exhibited decreased OSC after aging, it follows that the decrease in OSC can be expected to affect the selectivity of NO_x reduction. As outlined above, this can occur on the basis that: (i) a decrease in stored oxygen should result in an increased reductant concentration in the gas front during rich purging, favoring the formation of NH_3 over N_2, and (ii) less stored oxygen will be available in the rear of the catalyst to react with initially formed NH_3 to give N_2. In this context, it is instructive to examine the outlet CO profile during cycling (Fig. 13). As shown, CO slip was observed in all cases during rich purging, indicative of complete consumption of the stored oxygen. Similar to the NH_3 measured in the effluent, the amount of CO in the effluent decreased with increasing OSC, consistent with the role of stored oxygen in consuming reducing species such as CO and NH_3 in the catalyst.

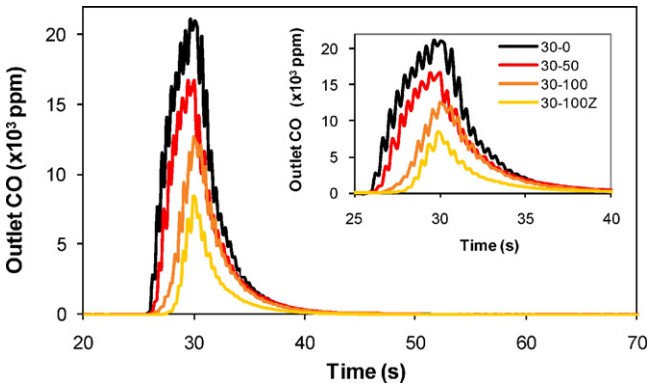

Fig. 13. Outlet CO concentration profiles during rich purge at 350 °C (inset: expanded view).

Finally, it is worth noting that a lengthening of the NO_x storage–reduction (NSR) zone may contribute to the observed increase in selectivity to NH_3 after aging. A recent study employing SpaciMS suggests that the longer the NSR zone (i.e., axial LNT portion where NO_x is stored and reduced), the shorter the downstream OSC-only zone (i.e., axial LNT portion free of stored NO_x) [66]. This leads to decreased oxidation of NH_3, slipping from the upstream NSR-zone, by oxygen stored in the OSC-only zone. Based on the results in the present study, we can reasonably argue that as the catalyst ages, the length of the NO_x storage–reduction zone increases, i.e., more catalyst length is used, since there are fewer active sites available per unit of catalyst volume. Consequently, more NH_3 escapes from the LNT without being oxidized.

In summary, it is clear that there are many factors which can account for the change in NO_x reduction selectivity after LNT aging, and further investigation of this subject is warranted.

4. Conclusions

It is generally agreed that the functioning of LNT catalysts involves four sequential steps [67]: (i) NO oxidation to NO_2, (ii) NO_x storage, (iii) NO_x release (i.e., nitrate decomposition) and (iv) NO_x reduction. In this study it was found that simulated road aging resulted in significant deterioration of catalyst performance in steps (ii), (iii) and (iv). For catalyst 30-0, containing no ceria, the decline in NO_x conversion after aging could be attributed mainly to the deterioration in cycle-averaged NO_x storage efficiency, which in turn is determined by the intrinsic NO_x storage efficiency and the extent to which the catalyst is regenerated during rich purging. In the case of 30-0, both of these properties were severely degraded, i.e., steps (ii) and (iii) no longer proceeded with high efficiency. In the case of aged ceria-containing catalysts, high cycle-averaged NSE was retained at 250 and 350 °C, the modest declines in NO_x conversion observed being attributable largely to increased rich phase NO_x release. In contrast, at 150 and 450 °C, poor cycle-averaged NSE associated with respectively loss of rich phase regeneration efficiency and intrinsic NSE was mainly responsible for significant declines in overall NO_x conversion.

After aging, all of the catalysts showed increased selectivity to NH_3 in the temperature range 250–450 °C. This can be explained on the basis that, relative to the fresh catalysts, the higher ratio of reductant to stored NO_x for the aged catalysts (due to their lowered NSE) should result in increased production of NH_3 versus N_2. However, a number of other factors are likely to play a role, including the slower rate of catalyst regeneration (due to PM sintering and Pt-Ba phase segregation), decreased catalyst OSC and lengthening of the NO_x storage–reduction zone.

Analytical data for the aged catalysts reveal two main physical changes which can explain the degradation in LNT performance. First, residual sulfur was observed in the catalyst washcoats. According to TEM and XPS data, sulfur was present as $BaSO_4$, thereby decreasing catalyst NO_x storage capacity and negatively affecting step (ii) above. Secondly, sintering of the precious metals in the washcoat was observed, which can be expected to lessen the contact between the Ba and PM phases, resulting in less efficient NO_x spillover from Pt to Ba during NO_x adsorption (and hence decreased NSE). Similarly, decreased rich phase nitrate decomposition suggests that Pt-Ba phase segregation adversely affected the rate of reductant spillover from Pt to Ba, while increasing rich phase NO_x slip is consistent with a decrease in the rate of the reverse NO_x spillover process and/or the intrinsic rate of PM-catalyzed NO_x reduction.

Finally, this study shows the spectacular improvement in LNT durability which can be achieved through the incorporation of CeO_2 or CeO_2-ZrO_2 (particularly the latter). Several factors are believed to be responsible, viz.:

(i) Ceria can be directly involved in NO_x storage/reduction as a supplement to the main NO_x storage component (Ba); hence, even if the NO_x storage capacity of the $Pt/BaCO_3/Al_2O_3$ component is degraded as a result of aging, NO_x storage can still proceed on the $Pt/CeO_2(\text{-}ZrO_2)$ component. Similarly, the $Pt/CeO_2(\text{-}ZrO_2)$ component can contribute to NO_x reduction.
(ii) Unlike the $Pt/BaCO_3/Al_2O_3$ component, for which segregation of the Pt and $BaCO_3$ can occur during aging, migration and sintering of Pt in the $Pt/CeO_2(\text{-}ZrO_2)$ component cannot lead to phase segregation, i.e., the Pt and $CeO_2(\text{-}ZrO_2)$ remain in intimate contact, which should be beneficial for the retention of NO_x storage efficiency, as well as efficient NO_x release.
(iii) Ceria-containing catalysts exhibit superior sulfation and desulfation characteristics as compared to their non-ceria analogs; more particularly, the ability of ceria to trap sulfur results in decreased sulfur accumulation on the main Ba NO_x storage component.

Acknowledgement

The authors thank Shelley Hopps for sulfur measurements, and Rob Spicer and Tonya Morgan for assistance with the rapid aging experiments. This project was funded by the U.S. Department of Energy (DOE) under award No. DE-FC26-05NT42631. However, any opinions, findings, conclusions, or recommendations expressed herein are those of the authors and do not necessarily reflect the views of the DOE.

References

[1] N. Miyoshi, S. Matsumoto, K. Katoh, T. Tanaka, J. Harada, N. Takahashi, K. Yokota, M. Sugiura, K. Kashahara, SAE Technical Paper Series, 950809 (1995).
[2] C. Enderle, C. Schoen, T. Ried, W. Mueller, L. Ruwisch, M. Koegel, S. Franoschek, T. Kreuzer, E. Lox, SAE Technical Paper Series, SP-1759 (2003).
[3] J. Breen, M. Marella, C. Pistarino, J.R.H. Ross, Catal. Lett. 80 (2002) 123.
[4] K. Yamamoto, R. Kikuchi, T. Takeguchi, K. Eguchi, J. Catal. 238 (2006) 449.
[5] N. Takahashi, A. Suda, I. Hachisuka, M. Sugiura, H. Sobukawa, H. Shinjoh, Appl. Catal. B 72 (2007) 187.
[6] W.S. Epling, L.E. Campbell, A. Yezerets, N.W. Currier, J.E. Parks II, Catal. Rev. 46 (2004) 163.
[7] S. Elbouazzaoui, E.C. Corbos, C. Courtois, P. Marecot, D. Duprez, Appl. Catal. B 61 (2005) 236.
[8] H. Abdulhamid, E. Fridell, J. Dawody, M. Skoglundh, J. Catal. 241 (2006) 200.
[9] L. Lietti, P. Forzatti, I. Nova, E. Tronconi, J. Catal. 204 (2001) 175.
[10] F. Rohr, U. Gobel, P. Kattwinkel, S. Philipp, P. Gelin, Appl. Catal. B 70 (2007) 189.
[11] C. Courson, A. Khalfi, H. Mahzoul, S. Hodjati, N. Moral, A. Kiennemann, P. Gilot, Catal. Comm. 3 (2002) 471.
[12] S. Poulston, R.R. Rajaram, Catal. Today 81 (2003) 603.
[13] X. Wei, X. Liu, M. Deeba, Appl. Catal. B 58 (2005) 41.
[14] Z. Liu, J. Anderson, J. Catal. 228 (2004) 243.
[15] N. Fekete, R. Kemmler, D. Voigtländer, B. Krutzsch, E. Zimmer, G. Wenninger, W. Strehlau, J.A.A. van den Tillaart, J. Leyrer, E.S. Lox, W. Müller, SAE Technical Paper Series, 970746 (1997).
[16] D. Uy, A.E. O'Neill, J. Li, W.L.H. Watkins, Top. Catal. 95 (2004) 191.
[17] M. Casapu, J.D. Grunwaldt, M. Maciejewski, M. Wittrock, U. Göbel, A. Baiker, App. Catal. B 63 (2006) 232.
[18] D.H. Kim, Y.H. Chin, G.G. Muntean, A. Yezeretz, N.W. Currier, W.S. Epling, H.Y. Chen, H. Hess, C.H.F. Peden, Ind. Eng. Chem. Res. 45 (2006) 8815.
[19] M. Casapu, J.D. Grunwaldt, M. Maciejewski, A. Baiker, M. Wittrock, U. Göbel, S. Eckhoff, Top. Catal. 42–43 (2007) 3.
[20] S. Elbouazzaoui, X. Courtois, P. Marecot, D. Duprez, Top. Catal. 30/31 (2004) 493.
[21] R. Strobel, F. Krumeich, S.E. Pratsinis, A. Baiker, J. Catal. 243 (2006) 229.
[22] D.H. Kim, J.H. Kwak, J. Szanyi, S.D. Burton, C.H.F. Peden, App. Catal. B 72 (2007) 233.
[23] T.J. Toops, B.G. Bunting, K. Nguyen, A. Gopinath, Catal. Today 123 (2007) 285.
[24] K. Nguyen, H. Kim, B.G. Bunting, T.J. Toops, C.S. Yoon, SAE Technical Paper Series, 2007-01-0470 (2007).
[25] D.H. Kim, Y.H. Chin, J.H. Kwak, C.H.F. Peden, Catal. Lett. 124 (2008) 39.
[26] B.H. Jang, T.H. Yeon, H.S. Han, Y.K. Park, J.E. Yie, Catal. Lett. 77 (2001) 21.
[27] G.W. Graham, H.W. Jen, J.R. Theis, R.W. McCabe, Catal. Lett. 93 (2004) 3.
[28] K. Yamazaki, T. Suzuki, N. Takahasi, K. Yojota, M. Sugiura, Appl. Catal. B 30 (2001) 459.
[29] F. Basile, G. Fornasari, A. Grimandi, M. Livi, A. Vaccari, Appl. Catal. B 69 (2006) 58.
[30] S. Matsumoto, Y. Ikeda, H. Suzuki, M. Ogai, N. Myoshi, Appl. Catal. B 25 (2000) 115.
[31] E.C. Corbos, X. Courtois, N. Bion, P. Marecot, D. Duprez, Appl. Catal. B 80 (2008) 62.
[32] H.Y. Huang, R.Q. Long, R.T. Yang, Appl. Catal. B 33 (2001) 127.
[33] G. Centi, G. Fornasari, C. Gobbi, M. Livi, F. Trifiro, A. Vaccari, Catal. Today 73 (2002) 287.
[34] J.M. Clacens, R. Montiel, H. Kochkar, F. Figueras, M. Guyon, J.C. Beziat, Appl. Catal. B 53 (2004) 21.
[35] J. Theis, J. Ura, C. Goralski, Jr. H. Jen, E. Thanasiu, Y. Graves, A. Takami, H. Yamada, S. Miyoshi, SAE Technical Paper Series, 2003-01-1160 (2003).
[36] Y. Ji, T.J. Toops, M. Crocker, Catal. Lett. 127 (2009) 55.
[37] V. Easterling, Y. Ji, M. Crocker, J. Ura, J.R. Theis, R.W. McCabe, this issue of Catal. Today.
[38] Y. Ji, J. Choi, T.J. Toops, M. Crocker, M. Naseri, Catal. Today 136 (2008) 146.
[39] L. Xu, R. McCabe, W. Ruona, G. Cavataio, SAE Technical Paper Series, 2009-01-0285 (2009).
[40] J.-S. Choi, W.P. Partridge, C.S. Daw, Appl. Catal. A 293 (2005) 24.
[41] J.-S. Choi, W.P. Partridge, W.S. Epling, N.W. Currier, T.M. Yonushonis, Catal. Today 114 (2006) 102.
[42] V. Perrichon, L. Retailleau, P. Bazin, M. Daturi, J.C. Lavalley, Appl. Catal 260 (2004) 1.
[43] M. Eberhardt, R. Riedel, U. Gobel, J. Theis, E.S. Lox, Topics Catal. 30/31 (2004) 135.
[44] J. Kaspar, P. Fornasiero, M. Graziani, Catal. Today 50 (1999) 285.
[45] C.E. Hori, H. Permana, K.Y.S. Ng, A. Brenner, K. More, K.M. Rahmoeller, D. Belton, Appl. Catal. B 16 (1998) 105.
[46] F. Fajardie, J.-F. Tempere, J.-M. Manoli, O. Touret, G. Djéga-Mariadassou, Catal. Lett. 54 (1998) 187.
[47] G.W. Graham, H.-W. Jen, W. Chun, R.W. McCabe, J. Catal. 182 (1999) 228.
[48] G. Graham, H.W. Jen, W. Chun, H. Sun, X. Pan, R. McCabe, Catal. Lett. 93 (2004) 129.
[49] K.M. Adams, G.W. Graham, Appl. Catal. B 80 (2008) 343.
[50] Z. Zou, M. Meng, N. Tsubaki, J. He, G. Wang, X. Li, X. Zhou, J. Haz. Mater. 170 (2009) 119.
[51] J. Breen, M. Marella, C. Pistarino, J. Ross, Catal. Lett. 80 (2002) 123.
[52] A. Sassi, R. Noirot, C. Rigaudeau, G. Belot, et al. Proceedings of the 6th Congress on Catalysis and Automotive Pollution Control (CAPoC6), Topics Catal., vol. 30, 2004, p. 267.
[53] Y. Ji, C. Fisk, V. Easterling, M. Crocker, J.-S.Choi, manuscript in preparation.
[54] Y. Ji, T.J. Toops, U.M. Graham, G. Jacobs, M. Crocker, Catal. Lett. 110 (2006) 29.
[55] E. Rohart, V. Belliére-Baca, K. Yokota, V. Harlé, C. Pitois, Top. Catal. 42/43 (2007) 71.
[56] S. Bernard, L. Retailleau, F. Gaillard, P. Vernoux, A. Giroir-Fendler, Appl. Catal. B 55 (2005) 11.
[57] B.M. Weiss, E. Iglesia, J. Phys. Chem. C 113 (2009) 13331.
[58] A. Martínez-Arias, M. Fernández-García, A. Iglesias-Juez, A.B. Hungria, J.A. Anderson, J.C. Conesa, J. Soria, Appl. Catal. B 38 (2002) 151.
[59] R.D. Clayton, M.P. Harold, V. Balakotaiah, C.Z. Wan, Appl. Catal. B 90 (2009) 662.
[60] Y. Ji, T.J. Toops, M. Crocker, Catal. Lett. 119 (2007) 257.
[61] S. Philipp, A. Drochner, J. Kunert, H. Vogel, J. Theis, E.S. Lox, Top. Catal. 30/31 (2004) 235.
[62] I. Nova, L. Castoldi, L. Lietti, E. Tronconi, P. Forzatti, SAE Technical Paper Series, 2006-01-1368 (2006).
[63] A.F. Diwell, R.R. Rajaram, H.A. Shaw, T.J. Truex, Stud. Surf. Sci. Catal. 71 (1991) 139.
[64] Y. Nagai, T. Hirabayashi, K. Dohmae, N. Takagi, T. Minami, H. Shinjoh, S. Matsumoto, J. Catal. 242 (2006) 103.
[65] J.A. Pihl, J.E. Parks II, C.S. Daw, T.W. Root, SAE Technical Paper Series, 2006-01-3441 (2006).
[66] J.-S. Choi, W.P. Partridge, J.A. Pihl, C.S. Daw, Catal. Today 136 (2008) 173.
[67] L. Olsson, H. Persson, E. Fridell, M. Skoglundh, B. Andersson, J. Phys. Chem. B 105 (2001) 6895.